

PCCP

Accepted Manuscript



This is an *Accepted Manuscript*, which has been through the Royal Society of Chemistry peer review process and has been accepted for publication.

Accepted Manuscripts are published online shortly after acceptance, before technical editing, formatting and proof reading. Using this free service, authors can make their results available to the community, in citable form, before we publish the edited article. We will replace this *Accepted Manuscript* with the edited and formatted *Advance Article* as soon as it is available.

You can find more information about *Accepted Manuscripts* in the [Information for Authors](#).

Please note that technical editing may introduce minor changes to the text and/or graphics, which may alter content. The journal's standard [Terms & Conditions](#) and the [Ethical guidelines](#) still apply. In no event shall the Royal Society of Chemistry be held responsible for any errors or omissions in this *Accepted Manuscript* or any consequences arising from the use of any information it contains.

Cite this: DOI: 10.1039/c0xx00000x

www.rsc.org/xxxxxx

ARTICLE TYPE

Oxygen-participated Electrochemistry of New Lithium-rich Layered Oxides Li_3MRuO_5 ($\text{M} = \text{Mn}, \text{Fe}$)

S. Laha,^a S. Natarajan,^a J. Gopalakrishnan,^{*a} E. Morán,^b R. Sáez-Puche,^b M. Á. Alario-Franco,^{b,c} A. J. Dos Santos-Garcia,^b J.C. Pérez-Flores,^c A. Kuhn,^c F. García-Alvarado,^{*c}

Received (in XXX, XXX) Xth XXXXXXXXXX 20XX, Accepted Xth XXXXXXXXXX 20XX

DOI: 10.1039/b000000x

We describe the synthesis, crystal structure and lithium deinsertion/insertion electrochemistry of two new lithium-rich layered oxides, Li_3MRuO_5 ($\text{M} = \text{Mn}, \text{Fe}$), related to rocksalt based Li_2MnO_3 and LiCoO_2 . The $\text{Li}_3\text{MnRuO}_5$ oxide adopts a structure related to Li_2MnO_3 ($C2/m$) where Li and $(\text{Li}_{0.2}\text{Mn}_{0.4}\text{Ru}_{0.4})$ layers alternate along the c -axis, while the $\text{Li}_3\text{FeRuO}_5$ oxide adopts a near-perfect LiCoO_2 ($R-3m$) structure where Li and $(\text{Li}_{0.2}\text{Fe}_{0.4}\text{Ru}_{0.4})$ layers are stacked alternately. Magnetic measurements indicate for $\text{Li}_3\text{MnRuO}_5$ the presence of Mn^{3+} and low spin configuration for Ru^{4+} where the itinerant electrons are occupying a π^* -band. The onset of a net maximum in the χ vs. T plot at 9.5 K and the negative value of the Weiss constant (θ) of -31.4 K indicate the presence of antiferromagnetic superexchange interactions according to different pathways. Lithium electrochemistry shows a similar behaviour for both oxides and related to the typical behaviour of Li-rich layered oxides where participation of oxide ion in the electrochemical processes is usually found. A long first charge process with capacities of 240 mAhg^{-1} (2.3 Li/f.u.) and 144 mAhg^{-1} (1.38 Li/f.u.) is observed for $\text{Li}_3\text{MnRuO}_5$ and $\text{Li}_3\text{FeRuO}_5$, respectively. An initial sloping region (OCV to ca. 4.1 V) is followed by a long plateau (ca. 4.3 V). Further discharge – charge cycling points to partial reversibility (ca. 160 mAhg^{-1} and 45 mAhg^{-1} for Mn and Fe, respectively). Nevertheless, just after a few cycles, cell failure is observed. X-ray photoelectron spectroscopy (XPS) characterisation of both pristine and electrochemically oxidized Li_3MRuO_5 reveals that in the $\text{Li}_3\text{MnRuO}_5$ oxide, Mn^{3+} and Ru^{4+} are partially oxidized to Mn^{4+} and Ru^{5+} in the sloping region at low voltage, while in the long plateau, O^{2-} is also oxidized. Oxygen release likely occurs which may be the origin of cells' failure on cycling. Interestingly, some other Li-rich layered oxides have been reported to cycle acceptably even with the participation of O^{2-} ligand in the reversible redox processes. In the $\text{Li}_3\text{FeRuO}_5$ oxide, the oxidation process appears to affect only to Ru ($4+$ to $5+$ in the sloping region) and O^{2-} (plateau) while Fe seems to retain its $3+$ state.

Introduction

There is a great interest to develop new cathode materials for Li-ion batteries based on rocksalt derived layered oxides related to LiCoO_2 and Li_2MnO_3 .^{1,2} We have recently explored two series of rock salt related oxides,^{3,4} $\text{Li}_3\text{M}_2\text{RuO}_6$ and Li_3MRuO_5 ($\text{M} = \text{Co}, \text{Ni}$), towards lithium deinsertion/insertion electrochemistry, of which the latter showed attractive specific capacities (ca. 200 mAhg^{-1}). The promising discharge capacities of the Li_3MRuO_5 ($\text{M} = \text{Co}, \text{Ni}$) presumably arise from (1) the lithium-rich layered rock salt structure similar to $\text{Li}(\text{Li}_{0.17}\text{Ni}_{0.25}\text{Mn}_{0.58})\text{O}_2$,⁵ (2) the redox characteristics of Co/Ru and Ni/Ru in these materials.³ and

(3) the participation of the oxide ions, O^{2-} , in the electrochemical processes. In view of the foregoing, we considered relevant to investigate other Li_3MRuO_5 compositions for $\text{M} = \text{Mn}$ and Fe. Herein we report the synthesis, structural and magnetic characterization and lithium deinsertion-insertion electrochemistry of these materials. We also report XPS characterisation of pristine and lithium-deinserted Li_3MRuO_5 ($\text{M} = \text{Mn}, \text{Fe}$). Finally, we compare the present results and those earlier reported on Li_3MRuO_5 ($\text{M} = \text{Co}, \text{Ni}$)³ and other Li-rich layered materials to draw a general conclusion. In the case of Li_3MRuO_5 the participation of oxide ions in the redox process seems to influence the electrochemical properties as expected by

the presence of Li in the transition metal (TM) layer. However, for this particular compound poor reversibility, probably due to enhanced oxygen loss, drive to cell failure on cycling in spite of the attractive high capacity developed in the first cycles.

5 Experimental

Synthesis

We attempted to prepare Li_3MRuO_5 for $M = \text{Mn}$ and Fe by the ceramic route involving solid state reaction of stoichiometric mixtures of Li_2CO_3 , $\text{MC}_2\text{O}_4 \cdot 2\text{H}_2\text{O}$ ($M = \text{Mn}, \text{Fe}$) and RuO_2 (pre-

10 dried overnight at 125°C). While we succeeded in preparing a single-phase LiCoO_2 -like $\text{Li}_3\text{FeRuO}_5$ by this method, we could not prepare the analogous Mn compound. However the Mn analogue was successfully prepared by the following method: first, Li_3RuO_4 precursor was prepared by reacting stoichiometric 15 quantities of Li_2CO_3 and RuO_2 .⁶ In the second step, Li_3RuO_4 was stoichiometrically mixed with $\text{MnC}_2\text{O}_4 \cdot 2\text{H}_2\text{O}$ and the mixture was reacted at 1250°C to obtain $\text{Li}_3\text{MnRuO}_5$ as single phase. The exact synthesis conditions are summarized in Table 1.

Table 1. Conditions for the synthesis of Li_3MRuO_5 ($M = \text{Mn}, \text{Fe}$).

Composition	Starting materials	Synthesis conditions ($^\circ\text{C}$, h)	Result
$\text{Li}_3\text{MnRuO}_5$	$\text{Li}_2\text{CO}_3 + \text{MnC}_2\text{O}_4 \cdot 2\text{H}_2\text{O} + \text{RuO}_2$	900, 12; 925, 12	$\text{Li}_2\text{MnO}_3 + \text{RuO}_2$
$\text{Li}_3\text{MnRuO}_5$	$\text{Li}_3\text{RuO}_4 + \text{MnC}_2\text{O}_4 \cdot 2\text{H}_2\text{O}$	900, 12; 1250, 24 (pellet), (*R)	$\text{Li}_3\text{MnRuO}_5$
$\text{Li}_3\text{FeRuO}_5$	$\text{Li}_2\text{CO}_3 + \text{FeC}_2\text{O}_4 \cdot 2\text{H}_2\text{O} + \text{RuO}_2$	900, 12; 925, 12 (*R)	$\text{Li}_3\text{FeRuO}_5$

*R indicates repeated heating with intermittent grinding at these conditions until the formation of the single phase.

25 Structural characterisation

Formation of single phase products and their crystal structures were studied by means of powder X-ray diffraction (PXRD). PXRD patterns were recorded with a PANalytical X'Pert diffractometer operated at 40 kV and 30 mA using Ni-filtered Cu 30 $K\alpha$ radiation. For Rietveld refinement, the data were collected in the 2θ range $5 - 90^\circ$ with a step size of 0.02° and step duration of 50 s. Rietveld refinements of the structures were carried out employing the program GSAS.⁷ A sixth order Chebychev polynomial for the background, zero, LP factor, scale, pseudo- 35 Voigt profile function (U, V, W and X), lattice parameters, atomic coordinates and B_{iso} (total 23 parameters) were used in the refinement. Thermal parameters were constrained to be the same for atoms occupying the same site. PXRD patterns were simulated using the program POWDERCELL.⁸

40 Magnetic characterisation

Magnetic susceptibility measurements were performed in a Quantum Design XL Squid magnetometer in the temperature range 2-300 K at 5 mT. The magnetic susceptibility data were collected after cooling the sample from room temperature to 2 K 45 in a zero field (ZFC) and after cooling in the measuring field (FC). Magnetization was measured at different temperatures in magnetic field strengths up to 5 T.

Electrochemical studies

Electrochemical characterisation of Li_3MRuO_5 ($M = \text{Mn}$ and Fe) 50 was carried out by galvanostatic and potentiostatic methods on

two electrode cells using a VMP3 system (BioLogic). Positive electrodes were prepared by mixing the corresponding active material, Li_3MRuO_5 , with a conductive carbon black (VULCAN XC-72 of Cabot Corp.) and a binder (Kynarfex, Elf Atochem) 55 in 85:10:5 weight ratio, respectively. Pellets of 8 mm diameter, having ≈ 17 mg of active material, were obtained by uniaxial pressing and drying at 80°C for overnight. Coin-type cells (CR2032) were assembled in an argon-filled glove box. A lithium disk was used as the negative electrode, 1M LiPF_6 in a 50:50 mixture of ethylene carbonate (EC): dimethyl carbonate (DMC) (LP30, Basf) as the electrolyte and a disk of glass-fiber paper (Whatman) as the separator.

Galvanostatic cycling properties were evaluated at constant current ($\approx C/20$ rate, being 20 the necessary hours to insert 1 Li/ 65 formula unit -f.u., hereafter-) in the 3.0 - 4.5 V potential range and at room temperature. Stepped-potential chronoamperometry (CA) experiments were performed in the same potential range by applying 10 mV every hour.

Synthesis of electrochemically deinserted $\text{Li}_{3-x}\text{MRuO}_5$ ($M = \text{Mn}$ 70 and Fe) samples was accomplished by potentiostatic charge up to selected potentials (see below) of lithium cells. Cells were kept at the selected potentials until the current fell below 5×10^{-4} mA in order to achieve equilibrium conditions.

X-ray photoelectron spectroscopy (XPS) characterisation

75 XPS measurements of the pristine materials and electrochemically oxidized samples, $\text{Li}_3\text{MnRuO}_5$ (4.15 and 4.50 V) and $\text{Li}_3\text{FeRuO}_5$ (3.80 and 4.50 V) were carried out with Kratos Axis Ultra DLD Spectrometer, using a focused monochromatised Al-K_α radiation (1486.708 eV). The pressure

inside the chamber was kept around 5×10^{-9} mbar during the measurements. The peak positions of all the spectra were corrected to the C1s core level peak at 284.6 eV. Core peaks were analyzed using non-linear Shirley-type background. The positions of the peaks and area under the curves were optimized by a weighted least-squares fitting method employing XPSpeak41 software.

Results and Discussion

Structural characterisation

The PXRD patterns of Li_3MRuO_5 ($M = \text{Mn}$ and Fe) are presented in Fig. 1. The PXRD patterns of $M = \text{Mn}$ and Fe indicate the formation of single phase rock salt related structures of Li_2MnO_3 and LiCoO_2 type, respectively.^{9, 10} In the LiCoO_2 ($R\bar{3}m$) structure, the cations are ordered in the octahedral sites of a cubic close packed (ccp) array of anions to give alternating (111) cubic planes of Li and Co atoms. The Li_2MnO_3 ($C2/m$) structure has the same stacking sequence of atoms, except that the transition metal layer now consists of both lithium and manganese [$\text{Li}_{1/3}\text{Mn}_{2/3}$], while the alternating lithium layer remains intact (the same as LiCoO_2). In the transition metal layer, both lithium and manganese are charge-ordered in two dimensions such that each Li is surrounded by six Mn atoms. The ordered presence of lithium atoms in the transition metal [$\text{Li}_{1/3}\text{Mn}_{2/3}$] layers reduces the symmetry of the overall Li_2MnO_3 structure to $C2/m$.

Considering the similarity of PXRD pattern of $\text{Li}_3\text{MnRuO}_5$ with Li_2MnO_3 ,⁹ we could refine the crystal structure of $\text{Li}_3\text{MnRuO}_5$ on the basis of the monoclinic Li_2MnO_3 ($C2/m$) model. The refined atomic coordinates and isotropic temperature factors are

Table 2. Atomic coordinates and isotropic displacement parameters (U_{iso}) for $\text{Li}_3\text{MnRuO}_5$. Space group $C2/m$, $a = 5.063(1)$ Å, $b = 8.639(1)$ Å, $c = 5.088(1)$ Å, $\beta = 109.41(1)^\circ$

Atom	site	x	y	z	U_{iso}	Occupancy
Li	2(b)	0	0.5	0	0.019(2)	0.585(4)
Mn	2(b)	0	0.5	0	0.019(2)	0.208(4)
Ru	2(b)	0	0.5	0	0.019(2)	0.208(4)
Li	2(c)	0	0	0.5	0.131(2)	1.0
Li	4(h)	0	0.319(1)	0.5	0.085(1)	0.959(2)
Mn	4(h)	0	0.319(1)	0.5	0.085(1)	0.021(2)
Ru	4(h)	0	0.319(1)	0.5	0.085(1)	0.021(2)
Li	4(g)	0	0.168(2)	0	0.038(1)	0.050(9)
Mn	4(g)	0	0.168(2)	0	0.038(1)	0.476(9)
Ru	4(g)	0	0.168(2)	0	0.038(1)	0.476(9)
O	4(i)	0.224(1)	0	0.225(1)	0.039(1)	1.0
O	8(j)	0.253(1)	0.325(1)	0.228(1)	0.028(1)	1.0

Reliability Factors: $R_p = 6.97\%$, $R_{wp} = 9.79\%$, $R_f2 = 10.70\%$, $\chi^2 = 2.13$

presented in Table 2, the bond lengths in Table 3 while the final Rietveld profile fit is shown in Figure 2.

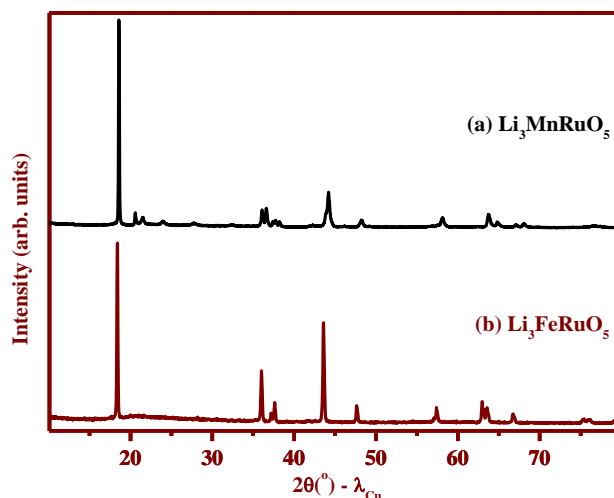


Fig. 1 PXRD patterns of (a) $\text{Li}_3\text{MnRuO}_5$ and (b) $\text{Li}_3\text{FeRuO}_5$

Cite this: DOI: 10.1039/c0xx00000x

www.rsc.org/xxxxxxx

ARTICLE TYPE

Table 3 Bond distances (Å) for $\text{Li}_3\text{MnRuO}_5$

	Bond length / Å	BVS
Li/Mn/Ru(2b) – O(4i)	2.080(1)×2	Li: 1.16 ; Mn: 2.57; Ru: 3.14
– O(8j)	2.071(2)×4	
Li(2c) – O(4i)	2.074(4)×2	Li: 1.02
– O(8j)	2.151(3)×4	
Li/Mn/Ru(4h)– O(8j)	1.968(1)×2	Li: 1.04 ; Mn: 2.32 ; Ru: 2.84
– O(8j)	2.178(1)×2	
– O(4i)	2.248(1)×2	
Li/Mn/Ru(4g) – O(4i)	1.963(1)×2	Li: 1.57 ; Mn: 3.48 ; Ru: 4.25
– O(8j)	1.953(1)×2	
– O(8j)	1.968(1)×2	

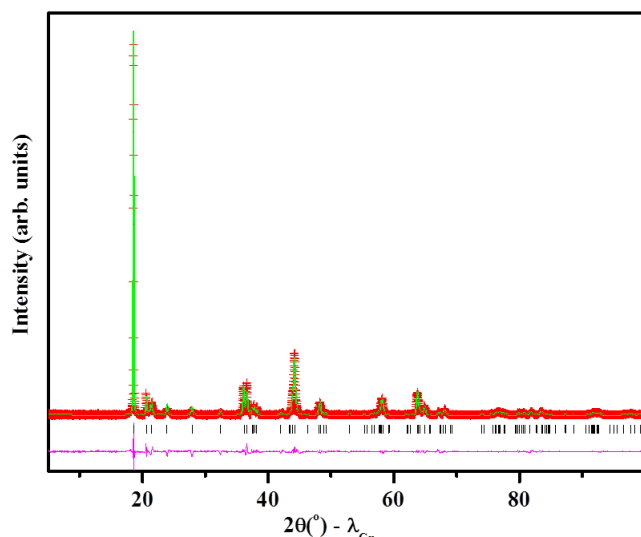
^a Footnote text.

Fig. 2 Rietveld refinement of the structure of $\text{Li}_3\text{MnRuO}_5$ from PXRD data on the basis of Li_2MnO_3 model. Observed (+), calculated (-) and difference (bottom) profiles are shown. The vertical bars indicate positions of the Bragg reflections

In the Li_2MnO_3 structure (shown in Fig. 3) there are three different Li positions, namely Li_{2b} , Li_{2c} and Li_{4h} (the subscripts represent corresponding Wyckoff sites) and a Mn position (Mn_{4g}).⁹ Out of the three different lithium atoms, Li_{2c} and Li_{4h} along with oxygen build the sheets of LiO_6 octahedra, while Li_{2b} and Mn_{4g} contribute for the sheets of $\text{Li}_{0.33}\text{Mn}_{0.67}\text{O}_6$ octahedra (sometimes referred as LiMn_2 layer). As above mentioned, in the transition metal layer, both lithium and manganese are charge-

ordered in two dimensions such that each Li is surrounded by six Mn atoms. These two sheets of octahedra are stacked alternately along the crystallographic *c*-direction of Li_2MnO_3 . Our refinement for $\text{Li}_3\text{MnRuO}_5$ indicates that Li_{2c} and Li_{4h} positions of Li_2MnO_3 are mainly occupied by lithium, with a small amount (~4%) of mixing of transition metal ions at the 4h site (see Table 2). On the other hand the Li_{2b} position of Li_2MnO_3 in the LiMn_2 layer is partially occupied by both lithium and transition metal atoms (Mn and Ru) with a ~58% occupancy of lithium (ideally 60%) and a ~42%, (ideally 40%) by the transition metal atoms, Mn and Ru, to the same extent. The Mn_{4g} site of Li_2MnO_3 is mainly occupied by an equal percentage of the transition metals (Mn and Ru), ~48% each, and a small percentage, ~5%, by lithium. If we ignore the slight admixture of atoms, we could write the structure of $\text{Li}_3\text{MnRuO}_5$ as $\text{Li}[\text{Li}_{0.2}\text{Mn}_{0.4}\text{Ru}_{0.4}]\text{O}_2$ which compares with the $\text{Li}[\text{Li}_{0.33}\text{Mn}_{0.67}]\text{O}_2$ model of Li_2MnO_3 . Accordingly, the LiO_6 octahedral sheets are the same in both structures, but the alternating $[\text{Li}_{0.33}\text{Mn}_{0.67}]$ sheets in Li_2MnO_3 are replaced by $[\text{Li}_{0.2}\text{Mn}_{0.4}\text{Ru}_{0.4}]$ sheets in $\text{Li}_3\text{MnRuO}_5$. As compared to Li_2MnO_3 , $\text{Li}_3\text{MnRuO}_5$ shows an increase in the cell parameter as well as in the average bond lengths of $\text{Li}/\text{Mn}/\text{Ru}-\text{O}_6$ octahedra. The latter could reflect the larger ionic radii of Mn^{3+} (0.645 Å) and Ru^{4+} (0.62 Å) (the likely oxidation states as revealed by XPS results, see later) than Mn^{4+} (0.53 Å).

PXRD pattern of $\text{Li}_3\text{FeRuO}_5$ also showed formation of single phase with a similarity to the PXRD pattern of LiCoO_2 (JCPDS 44-0145). Accordingly, we refined the PXRD data of $\text{Li}_3\text{FeRuO}_5$ on the basis of the LiCoO_2 (*R-3m*) structural model.¹⁰ The refinement showed an almost ideal distribution of cations with a small (~2%) mixing: $[\text{Li}_{0.98}\text{Fe}_{0.01}\text{Ru}_{0.01}]_{3a}[\text{Li}_{0.22}\text{Fe}_{0.39}\text{Ru}_{0.39}]_{3b}\text{O}_2$.

Cite this: DOI: 10.1039/c0xx00000x

www.rsc.org/xxxxxx

ARTICLE TYPE

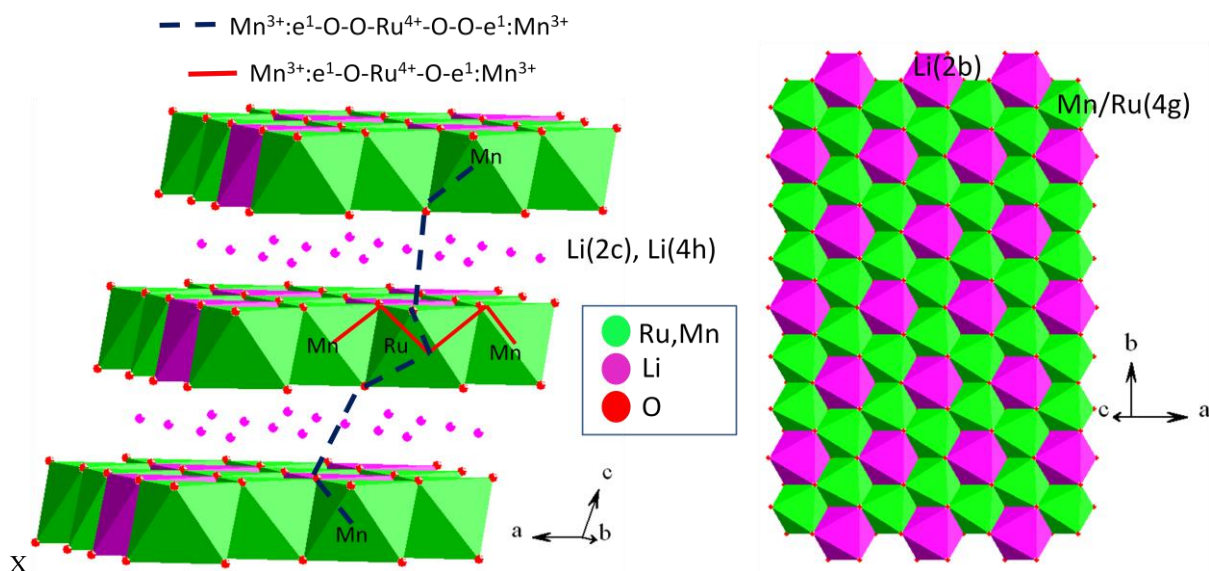


Fig. 3 Crystal structure of $\text{Li}_3\text{MnRuO}_5$ showing the Li_2MnO_3 type structure. (LiMn_2) layer is shown on the right. The analysis of the crystal structure of $\text{Li}_3\text{MnRuO}_5$, illustrating the different pathway through which superexchange interactions take place is depicted in the left hand side

5 Contrarily to $\text{Li}_3\text{MnRuO}_5$ in the transition metal layer Li, Fe and Ru are disordered as expected in the LiCoO_2 type structure. Refined atomic coordinates and isotropic temperature factors are given in Table 4 and bond lengths in Table 5. Thus, the structure of $\text{Li}_3\text{FeRuO}_5$ can be written as $\text{Li}[\text{Li}_{0.2}\text{Fe}_{0.4}\text{Ru}_{0.4}]\text{O}_2$ if we ignore
 10 the slight admixture of atoms. The final Rietveld profile fit is shown in Fig. 4 and its crystal structure in Fig. 5. Though the ionic radii of Co^{3+} (0.545 Å) and Fe^{3+} (0.55 Å) are similar in

octahedral environment, the presence of bigger Ru^{4+} (0.62 Å) and Li^+ (0.76 Å) in the mixed metal octahedral layers causes an
 15 increase in the cell parameters as well as in the average bond lengths as compared to the parent LiCoO_2 .^{10, 11} Both the $\text{Li}(3a)\text{--O}$ (2.128 Å) and $\text{Li/Fe/Ru}(3b)\text{--O}$ (2.036 Å) bonds are longer than the corresponding $\text{Li}(3a)\text{--O}$ (2.092 Å) and $\text{Co}(3b)\text{--O}$ (1.921 Å) bonds in LiCoO_2 .¹⁰

Table 4 Atomic coordinates and isotropic displacement parameters (U_{iso}) for $\text{Li}_3\text{FeRuO}_5$. Space group $R\bar{3}m$, $a = 2.931(1)$ Å, $c = 14.535(1)$ Å

Atom	site	x	y	z	U_{iso}	Occupancy
Li	3(a)	0	0	0	0.019(2)	0.981
Fe	3(a)	0	0	0	0.011(8)	0.013(1)
Ru	3(a)	0	0	0	0.011(8)	0.006(1)
Li	3(b)	0	0	0.5	0.019(2)	0.219
Fe	3(b)	0	0	0.5	0.027(1)	0.387(1)
Ru	3(b)	0	0	0.5	0.027(1)	0.394(1)
O	6(c)	0	0	0.245(1)	0.021(1)	1.0

Reliability Factors: $R_p = 5.87$, $R_{wp} = 7.95$, $R_f = 4.70$, $\chi^2 = 1.58$

25

Table 5 Bond distances (Å) and bond angles (°) for $\text{Li}_3\text{FeRuO}_5$

	Bond length / Å	BVS
Li/Fe/Ru(3a) – O	2.128(4)×6	Li: 1.00 ; Fe: 2.21; Ru: 2.71
Li/Fe/Ru(3b) – O	2.036(1)×6	Li: 1.29 ; Fe: 2.84 ; Ru: 3.48
Bond angle / °		
O(1) – Li/Fe/Ru(3a) – O(2)	87.06(1)	
O(1) – Li/Fe/Ru(3a) – O(3)	92.94(1)	
O(1) – Li/Fe/Ru(3b) – O(2)	92.06(1)	
O(1) – Li/Fe/Ru(3b) – O(3)	87.94(1)	

^a Footnote text.

Magnetic characterisation of pristine materials

Fig. 6 shows the evolution of the magnetic susceptibility with the temperature for $\text{Li}_3\text{MnRuO}_5$. It can be observed that the magnetic susceptibility obeys a Curie-Weiss law, $\chi = 0.40/T + 31.4$, over a wide temperature range, i.e. 300-30 K. The calculated effective magnetic moment takes the value of $4.44 \mu_B$, which is smaller than the theoretical expected one, $5.62 \mu_B$, for this compound, where the oxidation states are Ru^{4+} with low spin configuration t^4e^0 and $S=1$; while Mn^{3+} with $3d^4$ electronic configuration in octahedral coordination shows t^3e^1 with $S=2$. This discrepancy could be due to the low spin configuration of Ru^{4+} ; the electrons are itinerant and therefore their contribution to the magnetic moment will be very weak. A similar behaviour has been reported by Goodenough et al.¹² in the study of the magnetic properties of ruthenium perovskites of composition $\text{La}_2\text{MnRuO}_6$ where they indicated that the π -bonding 4d electrons of the low spin configuration of Ru^{4+} are occupying itinerant-electron states of a π^* -band. As consequence of this, the magnetic moment is mainly due to the Mn^{3+} ion. The negative value of -31.4 K of the Weiss constant is indicative of the onset of antiferromagnetic interactions. These antiferromagnetic interactions are fully confirmed from the net maximum found in the magnetic susceptibility at 9.4 K, see Figure 6.

In order to establish the origin of the divergence found between ZFC (zero field cooling) and FC (field cooling) magnetic susceptibility measurements below 9.4 K, magnetization as a function of the magnetic field has been performed at 4, 8 and 50 K and the hysteresis curve was measured at 4 K (Figure 7). A linear behaviour is observed above and below the critical temperature that agrees well with the antiferromagnetic behaviour proposed for the $\text{Li}_3\text{MnRuO}_5$ compound, where any metamagnetic transition is not observed below 5 T. The magnetic hysteresis loop obtained at 4 K (see Figure 7) indicates the absence of spin glass behaviour that will be rise a larger values of the FC magnetization than the ZFC data as a consequence of the freezing of the induced moment by the magnetic field. The weak ferromagnetic component arises from the canting of the Ru-Mn sublattices which are antiferromagnetically ordered through the superexchange pathways describe below.

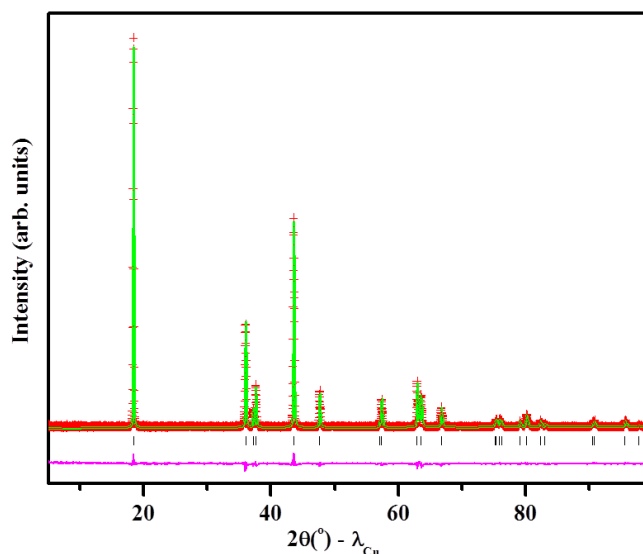


Fig.4 Rietveld refinement of the structure of $\text{Li}_3\text{FeRuO}_5$ from PXRD data on the basis of LiCoO_2 model. Observed (+), calculated (-) and difference (bottom) profiles are shown. The vertical bars indicate positions of the Bragg reflections

The analysis of the crystal structure of $\text{Li}_3\text{MnRuO}_5$, is very illustrative to establish the different pathways through which of these superexchange interactions take place (see Fig. 3). In this sense, in the *ab*-plane the antiferromagnetic superexchange interactions within the Ru-Mn layers following the pathway $\text{Mn}^{3+}:e^1\text{-O-Ru}^{4+}\text{-O-}e^1:\text{Mn}^{3+}$ should be stronger than the weak ferromagnetic ones expected for the $\text{Mn}^{3+}:e^1\text{-O-}e^0:\text{Ru}^{4+}$ because of π -itinerant electrons of the Ru^{4+} . Along the *c*-axis the pathway of the type $\text{Mn}^{3+}:e^1\text{-O-O-Ru}^{4+}\text{-O-O-}e^1:\text{Mn}^{3+}$ yields weak antiferromagnetic superexchange interactions. Both the low values of the Weiss constant and the estimated Neel temperature which are -33.4 K and 9.4 K, respectively, agree well with the weakness of these antiferromagnetic interactions that take place through the pathways mentioned above.

In the case of the $\text{Li}_3\text{FeRuO}_5$ the magnetic susceptibility exhibits a broad maximum around 300 K and a pronounced irreversibility

between the FC and ZFC susceptibility data that could be due to the presence of a ferromagnetic component arising from some iron oxide impurity not detected from XRD data. Figure 8 shows the temperature dependence of the magnetic susceptibility that follows a Curie-Weiss behaviour in the temperature range 100-30K and the obtained magnetic moment takes the value of $6.6\mu_B$ which fairly agrees the expected for Fe^{3+} ($S=5/2$) and Ru^{4+} ($S=1$). The negative value of $\theta=-17.7K$ and the onset of the net maximum found at 15K indicates the presence of antiferromagnetic interactions as in the case of the homologous Li_3MnRuO_5 compound. The value of 15 K estimated for the Néel temperature which is higher than 9.4 K found in the case of the Li_3MnRuO_5 could be explained as a consequence of the spin value of Fe^{3+} of $S=5/2$ higher than $S=2$ that shows the Mn^{3+} ion. From the results for both Li_3MRuO_5 compounds we formulate the pristine oxides as $Li_3M^{3+}Ru^{4+}O_5$ ($M = Mn$ and Fe) allowing for the interpretation of the electrochemical behavior regarding the role of the transition metals.

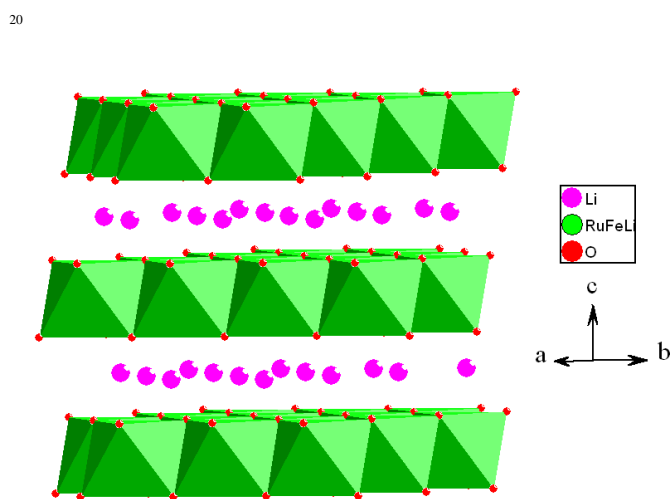


Fig. 5 Crystal structure of Li_3FeRuO_5 . For clarity, LiO_6 octahedra are omitted

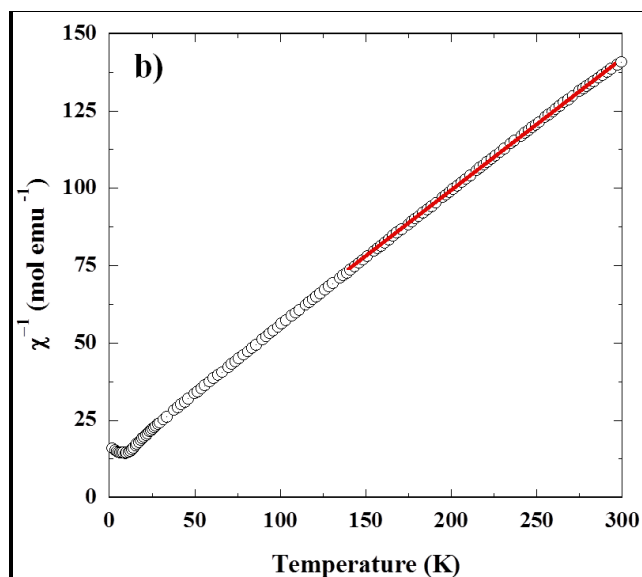
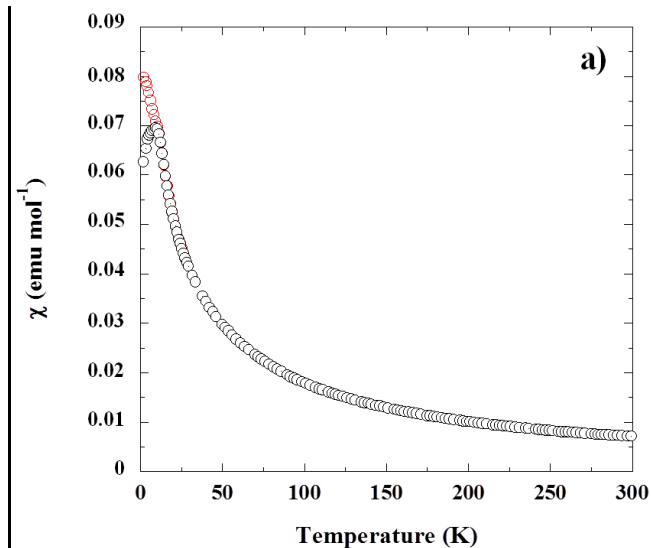


Fig. 6 a) Field cooling (red circles) and zero field cooling (black circles) magnetic susceptibility temperature dependence of Li_3MnRuO_5 , b) χ^{-1} vs. T plot

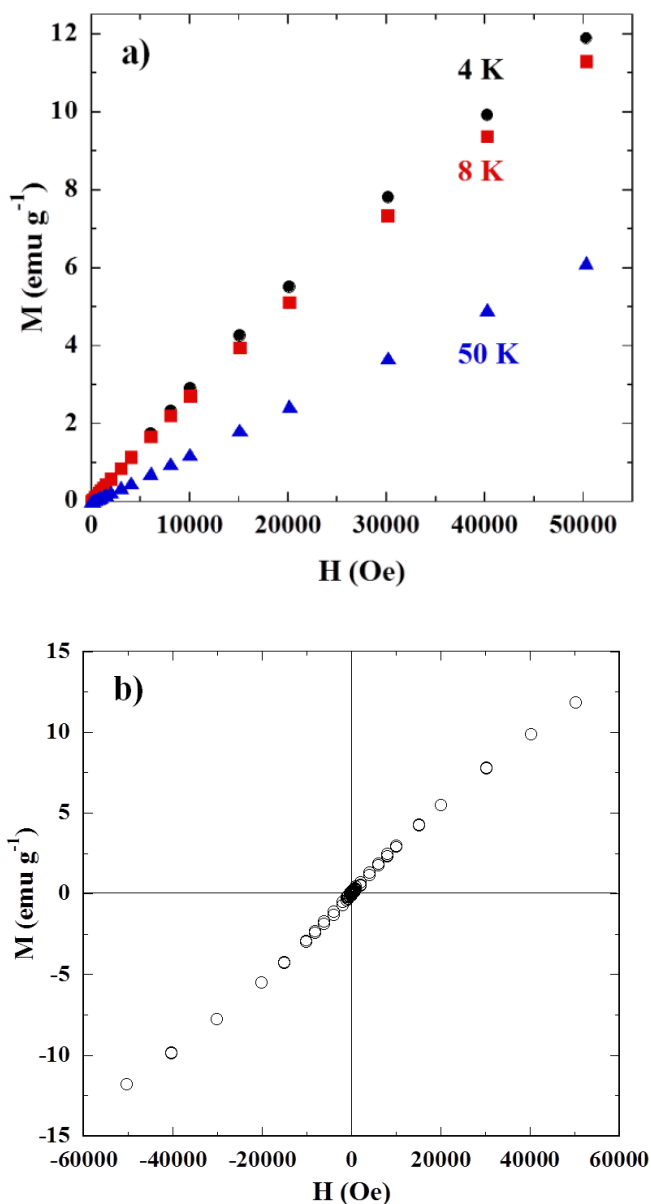


Fig. 7 a) Magnetization as a function of the magnetic field at 4, 8 and 50 K and b) the hysteresis curve measured at 4 K.

XPS of pristine materials

X-ray photoelectron spectroscopy (XPS) measurements were carried out on the pristine Li_3MRuO_5 ($M = \text{Mn}$ and Fe) oxides to determine the oxidation states of the metal atoms. The core level Ru 3d spectra exhibits Ru 3d_{5/2} binding energies (BE) around 282.0 and 281.8 eV for $\text{Li}_3\text{MnRuO}_5$ and $\text{Li}_3\text{FeRuO}_5$, respectively (Figures 9a and 10a and Table 6). In both oxides, the oxidation state of ruthenium corresponds to Ru^{4+} .¹³ The core level spectrum of Mn 2p_{3/2} in pristine $\text{Li}_3\text{MnRuO}_5$ shows a peak maximum at around 641.8 eV (Figure 9b and Table 6) which corresponds to Mn^{3+} .¹⁴ The core level peak of Fe 2p_{3/2} of $\text{Li}_3\text{FeRuO}_5$ appears at around 710.3 eV (Figure 10b and Table 6) which can be attributed to Fe^{3+} .¹⁵ On the other hand, O 1s core level spectra in the pristine samples exhibit two maxima each. The first peak (529.5 and 529.3 eV in $\text{Li}_3\text{MnRuO}_5$ and $\text{Li}_3\text{FeRuO}_5$, respectively)

in each spectrum corresponds to O^{2-} anions in a crystalline network and the second one, 531.4 eV in both samples (Figures 9c and 10c and Table 6), belongs to weakly adsorbed surface oxygen species.^{16, 17} These results, which are in full agreement with oxidation states obtained from magnetic characterisation, allow to formulate the pristine oxides as $\text{Li}_3\text{M}^{3+}\text{Ru}^{4+}\text{O}_5$ ($M = \text{Mn}$ and Fe) in order to interpret the electrochemical behaviour.

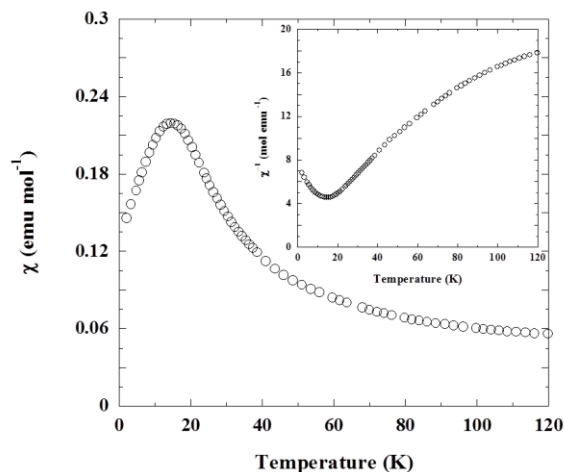


Fig. 8 Zero field cooling magnetic susceptibility temperature dependence of $\text{Li}_3\text{FeRuO}_5$, Inset shows χ' vs. T plot.

Electrochemical behaviour

$\text{Li}_3\text{MnRuO}_5$

Figure 11 shows the first two charge-discharge cycles of $\text{Li}_3\text{MnRuO}_5$ in the 3.0 to 4.5 V voltage range.

For $\text{Li}_3\text{MnRuO}_5$, an initial sloping region followed by a long plateau developing a total large capacity in the first charge (ca. 240 mAhg⁻¹) can be seen. The corresponding equivalent quantity of de-inserted lithium, ca. 2.3 Li/f.u., deserves attention, because it is higher than that expected for oxidation of Mn^{3+} to Mn^{4+} and Ru^{4+} to Ru^{5+} . The general behaviour is similar to that reported for Li-rich layered $\text{Li}[\text{Li}_{1-x}\text{M}_x]\text{O}_2$ oxides, in particular the solid solution $\text{Li}_2\text{MnO}_3\text{-LiMO}_2$ ($M = \text{Ni}, \text{Co}, \text{Cr}^{18-28}$). We observed a similar electrochemical behaviour in other members of the Li_3MRuO_5 series ($M = \text{Co}$ or Ni) as well.³ According to the structural characterisation above presented, $\text{Li}_3\text{MnRuO}_5$ can be expressed in fact as $\text{Li}[\text{Li}_{0.2}\text{Mn}_{0.4}\text{Ru}_{0.4}]\text{O}_2$ being isostructural to Li_2MnO_3 .

A significant amount of lithium ions (ca. 1.0 Li/f.u., 105 mAh/g) are de-inserted in the 3.0 - 4.25 V voltage range. According to the voltage profile in this region, it seems that more than one process are involved, both of them being ruled by solid solution formation. Considering the formula $\text{Li}_3\text{Mn}^{3+}\text{Ru}^{4+}\text{O}_5$, which has been proposed in view of magnetic and XPS characterization, the incomplete oxidation of both Mn^{3+} and Ru^{4+} to Mn^{4+} and Ru^{5+} , respectively, accounts for the partial de-insertion of lithium ions in this voltage region. Interestingly, the case is different from that recently reported for the solid solution $\text{Li}_2\text{MnO}_3\text{-Li}_2\text{RuO}_3$ ¹⁹ where Ru^{4+} and Mn^{4+} are present and therefore only Ru^{4+} is

active upon oxidation in this voltage range.

The presence of the two processes in $\text{Li}_3\text{Mn}^{3+}\text{Ru}^{4+}\text{O}_5$ is clearly seen in the voltammogram shown in Figure 11b. In the first oxidation wave, two peaks at 3.8 and 4.1 V are clearly seen.

5 These peaks can be assigned to $\text{Ru}^{4+}/\text{Ru}^{5+}$ and $\text{Mn}^{3+}/\text{Mn}^{4+}$ redox pairs, respectively, taking into account previous results on very related oxides. For example, Ru^{4+} to Ru^{5+} oxidations have been found to occur at 3.6 V in the very related cases of $\text{Li}_2\text{Ru}_{1-y}\text{M}_y\text{O}_3$ (M = Mn or Sn).^{19, 20} The Mn^{3+} to Mn^{4+} oxidation process has

10 been reported to occur at 4.0 V in LiMn_2O_4 .²⁹⁻³¹ Interestingly, the corresponding reduction peaks are clearly observed at 3.43 and 4.09 V. The almost negligible polarization of the high voltage peak at ca. 4 V seems to indicate that other processes may be occurring in the same voltage region, probably participated by
15 modification of the oxygen deposited species after electrolyte oxidation in the first oxidation and masking the corresponding peaks. Note that the reduction peak at 4.09 is very broad and flattened so that maximum is difficult to assign.

Table 6 XPS data for Li_3MRuO_5 , M = Mn and Fe at different oxidation stages.

Li_3MRuO_5	Conditions	Ru ($3d_{5/2}$) (eV)	M ($2p_{3/2}$) (eV)
	Pristine	282.0	641.8
M = Mn	Oxidized up to 4.15 V	282.4	642.2
	Oxidized up to 4.50 V	282.7	643.0
M = Fe	Pristine	281.8	710.3
	Oxidized up to 3.80 V	282.9	709.2
	Oxidized up to 4.50 V	283.0	--

20

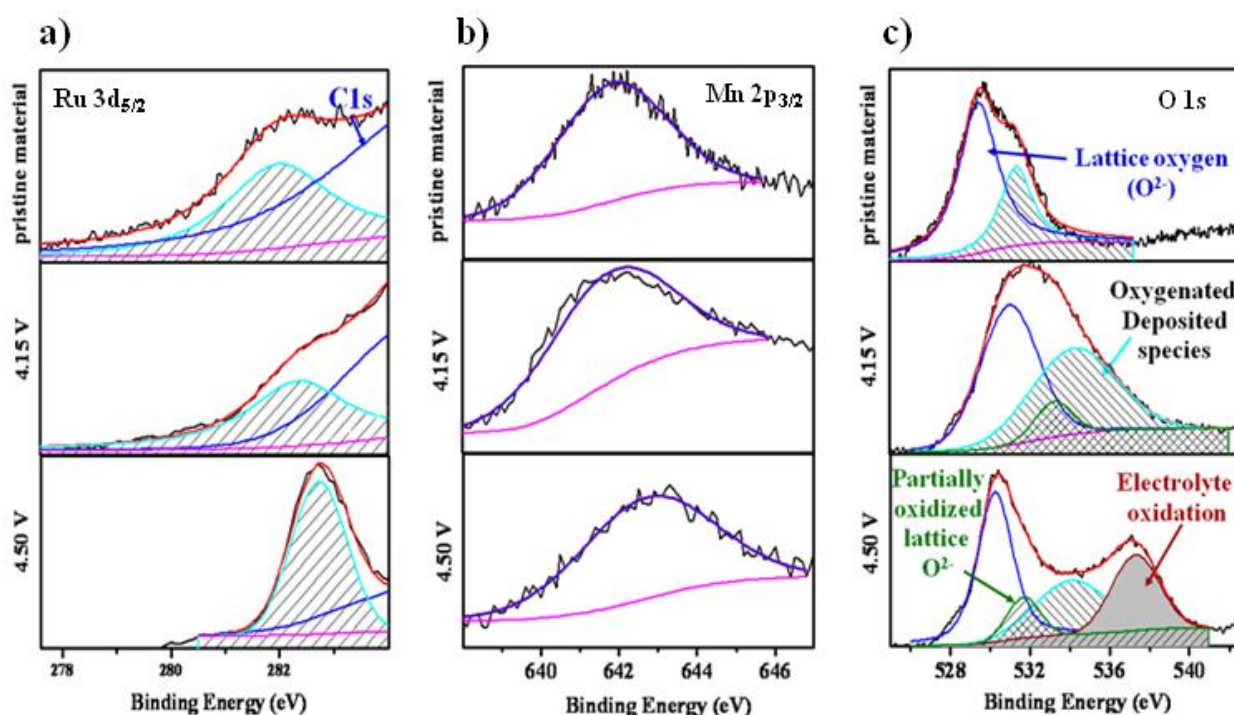


Fig. 9 Comparison of XPS data for pristine, 4.15 V and 4.50V oxidized $\text{Li}_3\text{MnRuO}_5$ samples. (a) Ru 3d spectra (b) Mn 2p spectra and (c) O 1s spectra. X

At even higher voltage another well differentiated region is observed between 4.25 and 4.4 V, according to voltage profile. A
25 large plateau indicates the occurrence of a new electrochemical process which is evidenced in the voltammogram shown in Fig.

11b, where a high oxidative current develops an incomplete peak at high voltage.

30

Cite this: DOI: 10.1039/c0xx00000x

www.rsc.org/xxxxxxx

ARTICLE TYPE

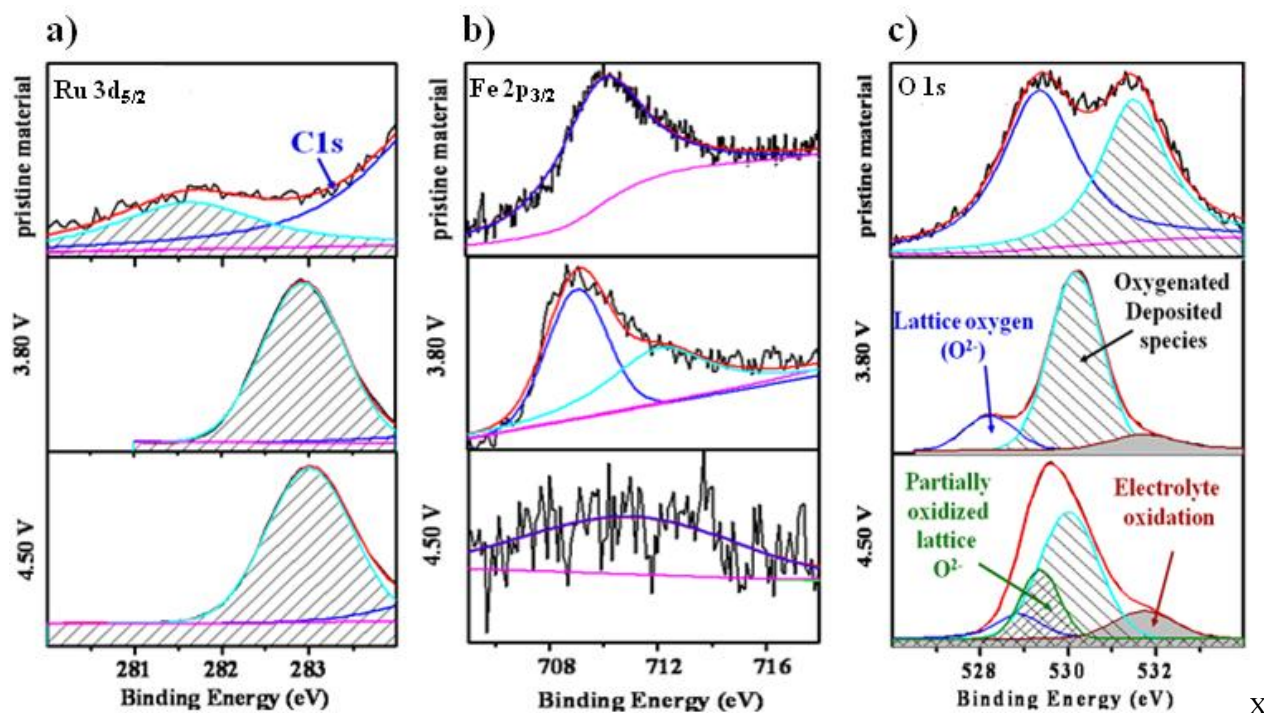


Fig. 10 Comparison of XPS data for pristine, 3.80 V and 4.50 V oxidized $\text{Li}_3\text{FeRuO}_5$ samples. (a) Ru 3d spectra (b) Mn 2p spectra and (c) O 1s spectra.

Much of the capacity developed during the first charge corresponds to this region in which ca. 1.3 Li ions seems to be de-inserted. Such a large amount of lithium may correspond to oxidation of Mn^{3+} or Ru^{4+} to high valence states, 5+ and 6+, respectively. In view of the high polarizing power of these cations, related to an increasing covalency of the M-O bond, another scenario involving the oxidation of lattice O^{2-} to O^- can be proposed. In this connection, the oxidation of the ligand, oxide ion, to O^- , has been reported in the closely related oxide $\text{Li}_2\text{Ru}_{0.5}\text{Mn}_{0.5}\text{O}_3$.¹⁹ The participation of the ligands in the redox chemistry was even early proposed in the deep de-lithiation of LiCoO_2 to CoO_2 .³² However, the oxidation of O^{2-} ligand involves oxygen evolution as a typical characteristic of lithium rich layered transition metal oxides of the solid solution Li_2MnO_3 - LiMO_2 where high valent cations are formed on oxidation.^{21, 23, 28}

To address the redox process involved in the deinsertion of lithium from $\text{Li}_3\text{MnRuO}_5$, XPS measurements were performed on both samples oxidized to two different voltages. The spectra for pristine $\text{Li}_3\text{MnRuO}_5$ above described and for samples charged up to 4.15 V and 4.50 V are shown in Figure 9 and Table 6. The Ru 3d_{5/2} core level spectrum which shows a binding energy ~282.0 eV for pristine $\text{Li}_3\text{MnRuO}_5$, consistent with Ru^{4+} ,¹³ shifts positive to 282.4 eV in sample oxidized at 4.15 V (Figure 9a and Table 6). This positive shift indicates likely oxidation of Ru^{4+} to Ru^{5+} in this oxidized sample. Electrochemical data showed that

oxidation of Ru^{4+} and Mn^{3+} in the low voltage region (3-4.25 V) was not completed. Thus, we also investigated the characteristic of the Ru 3d_{5/2} core level spectrum in the sample oxidized at 4.50 V. As expected, it can be seen an additional positive shift to 282.7 eV indicative of further oxidation of Ru^{4+} above 4.15 V. The situation is similar regarding Mn; the core level spectrum of Mn 2p_{3/2} in the pristine $\text{Li}_3\text{MnRuO}_5$ shows a peak maximum around 641.8 eV, which corresponds to Mn^{3+} (Figure 9b and Table 6).¹⁴ When the $\text{Li}_3\text{MnRuO}_5$ electrode is charged up to 4.15 V, the Mn 2p_{3/2} binding energy shifts positive to 642.2 eV and later to 643.0 eV at 4.50 V, suggesting an oxidation of Mn^{3+} to Mn^{4+} (Figure 9b and Table 4).¹⁴ Pristine $\text{Li}_3\text{MnRuO}_5$ shows two peaks for O 1s, first one at 529.5 eV (lattice oxide ion, O^{2-}) and 531.4 eV (weakly adsorbed surface species).^{16, 33} In the charged materials, the intensity and the area under the peak at ~531.4 eV increases. A new feature at ~537.3 eV appears, which likely corresponds to electrolyte oxidation.^{17, 33} In the 4.50 V oxidized material, a new component around 531.6 eV appears and this is likely to be due to partially oxidized lattice oxide (with a lower electron density as compared to O^{2-} in the pristine material) (Figure 9c).³³ The results indicate a progressive oxidation of the transition metals to Mn^{4+} and Ru^{5+} . At 4.15 V, metal oxidation has not been completed yet as expected from the electrochemical curve while partial electrolyte oxidation has started. At some point below 4.50 V, the ideal composition $\text{LiMn}^{4+}\text{Ru}^{5+}\text{O}_5$ in the fully charged state is reached, while extra capacity is developed due to oxide lattice oxidation.

Now, paying attention to the discharge, it can be seen that capacity drops and voltage profile is more similar to those of the region in which oxidation of Mn and Ru occurs though a high voltage contribution is observed. Second charge parallels the voltage profile of the discharge showing the reversibility onwards.

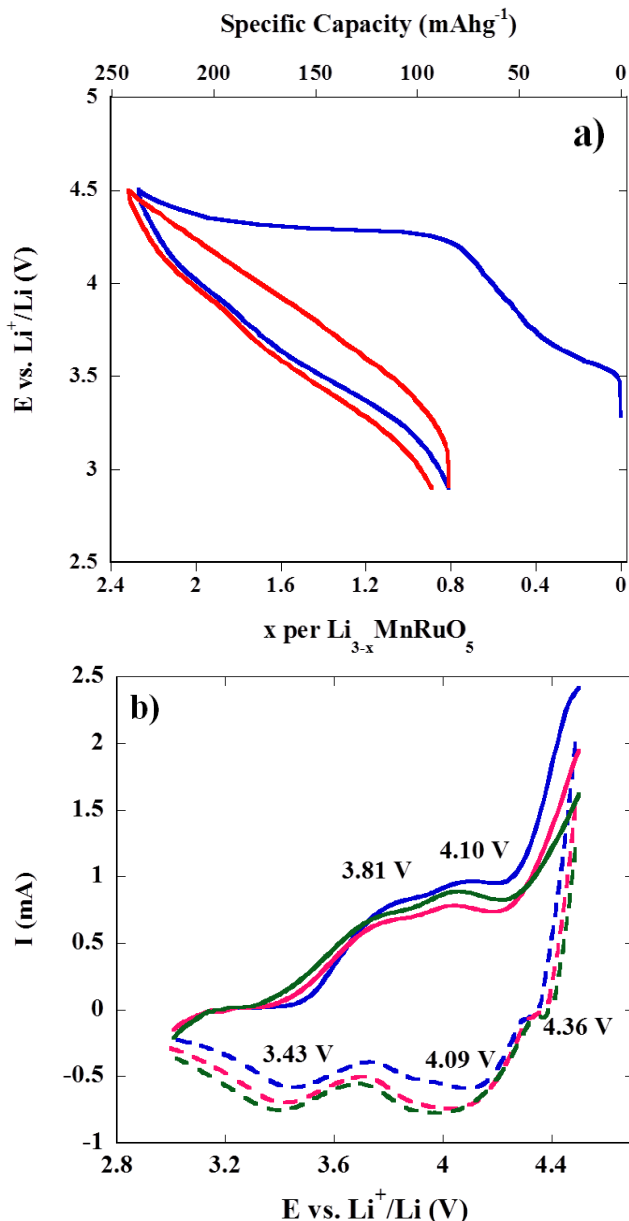


Fig. 11 a) Typical voltage-composition/capacity plot showing first (blue) and second (red) charge-discharge cycles of cell bearing Li₃MnRuO₅ as the active material. b) Stepped-potential chronoamperometry plot of Li₃MnRuO₅ electrode (10 mV/h). Oxidation and corresponding reduction cycles are plotted in continuous and dashed line, respectively.

Thus, we note that the reversible capacity (ca. 160 mAhg⁻¹, 1.55 Li p.f.u.) observed after the first charge is not only due to Mn⁴⁺ and Ru⁵⁺ reduction/oxidation (only ca. 1.0 Li/f.u., 105 mAhg⁻¹ were ascribed to these cations on the first charge in the 3.0 - 4.25 V voltage range) but also to a reversible contribution at high voltage of the O⁻ / O²⁻ redox couple. The voltammogram shown in Fig. 11b shows that after the first oxidative wave, the high

current observed at high voltage ascribed to the O⁻ / O²⁻ redox couple, decreases considerably while in the reductive wave, the oxide ion related process is observed as a peak of current at 4.36 V that keeps the same current in the three cycles shown.

However, it seems clear from the voltage profile that the two phase transformation taking place during the long plateau of the first charge is not reversible. This can be due to a significant irreversible loss of oxygen that is associated with oxygen vacancies and structural reorganization as it has been proved in the case of Li₂Ru_{1-y}Sn_yO₃. In the latter, oxygen evolution is partially inhibited by the presence of Sn facilitating the condensation of O⁻ to O₂²⁻ and hence favouring reversibility.²⁰

Li₃FeRuO₅

Figure 12a shows the first two charge-discharge cycles of Li₃MnRuO₅ in the 3.0 to 4.5 V voltage range. The behavior resembles the one described for the Mn analog inasmuch as a long charge process (ca. 144 mAhg⁻¹, 1.38 Li/f.u.), in which at least three voltage-composition regions are distinguished, is followed by a sloping reversible discharge shorter than first charge. In the beginning of the first charge, a sloping region between 3.0 and 4.0 V can be identified in the voltage-composition curve. The process is clearly defined at 3.7 V in the voltammogram of Fig. 12b. The potential indicates that in this voltage region Ru⁴⁺ is being oxidized.

The capacity developed in this region (ca. 50 mAhg⁻¹) is half of that in the case of Mn compound and corresponds to ca. 0.45 Li/f.u. Note that according to XPS characterisation, the pristine material can be expressed as Li₃Fe³⁺Ru⁴⁺O₅. As in the case of Li₃MnRuO₅, oxidation of Ru⁴⁺ is not completed at this stage. Besides, the second electroactive metal is now Fe³⁺ which is not expected to be oxidized at such low voltage.

A large capacity process occurs above 4.0 V involving a long plateau at ca. 4.2 V. Similarly to the case of Mn, we could ascribe this to the oxidation of oxide ions. The oxidative process is detected also in voltammogram shown in Fig. 12b as a broad peak at 4.26 V. Finally at ca. 4.5 V, another process is detected in the voltage-composition curve (Fig. 12a). Whether it is related with the electrolyte catalyzed oxidation due to the presence of an impurity no detectable by conventional XRD remains unknown. Note that magnetic measurement detected the presence of a small amount of strongly ferromagnetic impurity. We also noted that the extension and appearance of this process depends somehow on the batch. For example in the experiment shown in Fig. 12b this high voltage process is not detected. However, the oxidation of Fe³⁺ in Li₃Fe³⁺Ru⁴⁺O₅ is discarded since it is expected at much higher voltage according to previous results on related materials (ca. 5.1 V³⁴). In any case we discarded also this possibility based on XPS experiments (see below).

On discharge, again similarly to the Mn case, a sloping discharge shorter than charge and partially reversible can be seen (Fig. 12a). After first charge, the capacity is mainly due to the Ru⁵⁺/Ru⁴⁺ redox couple, but with participation of O⁻/O²⁻ as indicated by the maxima of negative current located at 4.10 V (Fig. 12b). Thus, oxidation of O²⁻ seems to be also reversible to some extent.

On the other hand, we did not investigate oxidation of Fe³⁺ at ~5 V, due to the instability of the electrolyte at such high voltage.

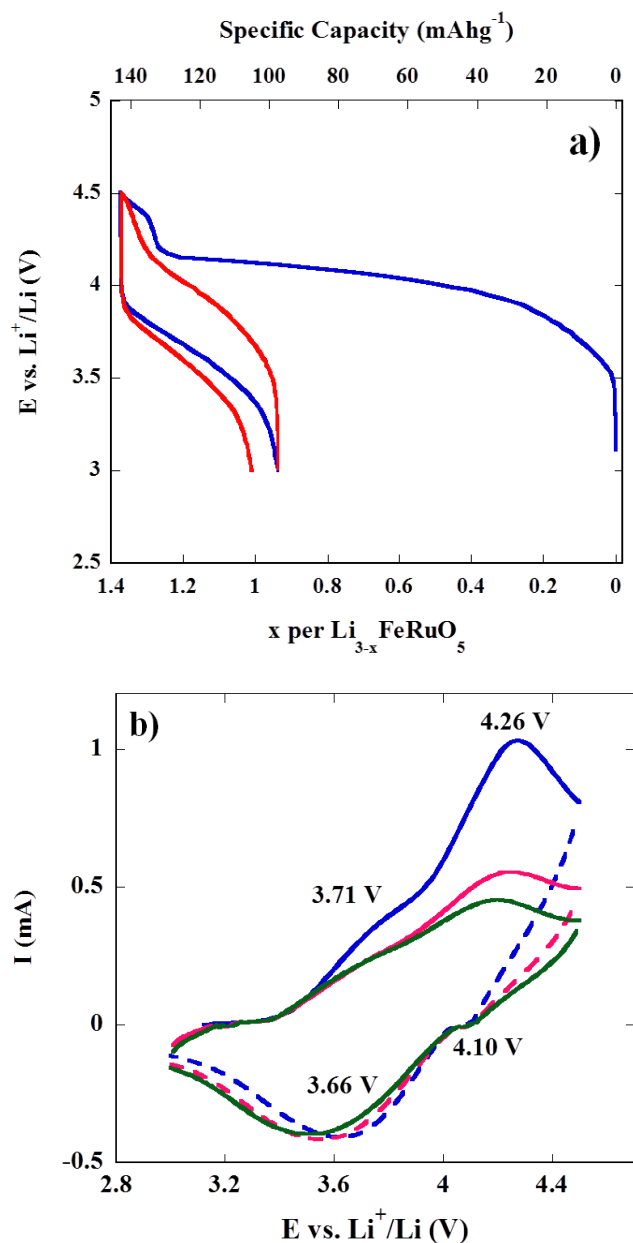


Fig. 12 a) Typical voltage-composition/capacity plot showing first (blue) and second (red) charge - discharge cycles of cell bearing $\text{Li}_3\text{FeRuO}_5$ as the active material. b) Stepped-potential chronoamperometry plot of $\text{Li}_3\text{FeRuO}_5$ electrode (10 mV/h). Oxidation and corresponding reduction cycles are plotted in continuous and dashed line, respectively

To confirm this interpretation of the electrochemical behaviour of $\text{Li}_3\text{FeRuO}_5$, we recorded XPS spectra for samples charged up to 3.80 V and 4.50 V. Data are shown in Figure 10 and Table 6 together with those of pristine $\text{Li}_3\text{FeRuO}_5$. The core level spectrum of Ru $3d_{5/2}$ in $\text{Li}_3\text{FeRuO}_5$, shifts positive by more than 1 eV, from 281.8 eV in the pristine material to 282.9 eV, when oxidized up to 3.80 V. This shift reveals that Ru^{4+} is oxidized to higher oxidation states (Figure 10a and Table 6). A further, but very small, shift to 283.0 eV when oxidized at 4.50 V indicates that oxidation of Ru^{4+} mainly occurs below 3.8 V. Note that the

corresponding process was observed by electrochemical methods close to 3.6 V and that capacity indicated that oxidation of Ru^{4+} was not completed at 4.0 V. Fe $2p_{3/2}$ core spectrum, which occurs at 710.3 eV, corresponding to Fe^{3+} ,¹⁵ in the pristine material shifts negative to 709.2 eV upon oxidation to 3.8 V and a weak satellite appears around 712.2 eV, besides. When oxidized to 4.50 V, no clear peak is observed. Both effects could result from a modification of the oxygen ligands around iron inducing strong electronic redistributions in the Fe-O bonds. A similar explanation has been given by Sathiyaraj et al.¹⁷ Nevertheless, we may discard oxidation of Fe^{3+} below 4.5 V. The O 1s spectrum for the pristine $\text{Li}_3\text{FeRuO}_5$ exhibits the two well resolved characteristic features at 529.3 eV and 531.4 eV, corresponding to lattice oxide, O^{2-} , as previously described.^{16, 33} As the pristine $\text{Li}_3\text{FeRuO}_5$ is charged to 3.80 V, the peaks shift negative and a new feature appears at around 531.7 eV due to electrolyte oxidation.^{17, 33} On further oxidation to 4.50 V, a new peak around 529.4 eV comes into picture, corresponding to oxidized O^{2-} ions as in the case of $\text{Li}_3\text{MnRuO}_5$.³³ The results reveal that Ru^{4+} is definitely getting oxidized to Ru^{5+} in the samples charged to 3.80 V though we do not have a conclusive evidence of the oxidation state of iron and oxygen in the oxidized samples. It is most likely that iron remains in the Fe^{3+} state with a reorganization of oxygen accompanying the oxygen release due to oxidation of part of oxide ions.

Cycling behavior of Li_3MRuO_5

The first charge capacity is developed through the partial oxidation of both Mn^{3+} and Ru^{4+} for $\text{M} = \text{Mn}$ and Ru^{4+} for $\text{M} = \text{Fe}$ compound, followed by the partial oxidation of O^{2-} to O^- ions. On discharge, electrochemical characterisation suggests that the above mentioned cations are reduced as well as O^- at least partially. Similar partial reversible behaviour of the O^{2-}/O^- redox couple has been previously shown in very related layered compounds such as $\text{Li}_2\text{Ru}_{1-y}\text{Mn}_y\text{O}_3$ ^{19, 20} and $\text{Li}_2\text{Ru}_{1-y}\text{Sn}_y\text{O}_3$.¹⁶ We also proposed a role of this redox couple in the electrochemical behavior of other members of the Li_3MRuO_5 family ($\text{M} = \text{Co}$ and Ni) that behaves quite similarly.³

However, long cycling behaviour is found to be limited in all the Li_3MRuO_5 investigated compounds. After first charge, reversibility is observed and capacity is well kept (Figure 13) but just for a few cycles. The figure shows the last cycle number before electrical failure occurs as a characteristic of every cell when cycling these materials up to 4.50 V. We believe that contrarily to that observed for related systems where long life cycling was achieved with the participation of a reversible anionic redox system,¹⁹⁻²¹ in the case of the Li_3MRuO_5 series, oxygen evolution is likely not inhibited by reorganization of oxygen environments based on the formation of O_2^{2-} as in other systems. In fact, if the participation of the O^{2-} ligand in the redox process is minimised by cycling Li_3MRuO_5 in narrower voltage range, cyclability is very much improved. Compare for example data corresponding to $\text{M} = \text{Mn}$ cycled up to 4.15 and 4.50 V depicted in Fig. 13. At this lower cut-off voltage, the cycling is improved and cell life is longer with very good capacity retention, albeit lower capacity is reached due the shortening of

the voltage range.

Cycling life of cells is short in both cases, because, cell failure is observed just after few cycles in the 3.0–4.5 V range. It seems then that accommodation of oxidized oxygen species in Li_3MRuO_5 is neither favoured in the LiCoO_2 structure of $\text{Li}_3\text{FeRuO}_5$ nor in the Li_2MnO_3 structure of $\text{Li}_3\text{MnRuO}_5$, resulting in poor cycling behaviour. Interestingly, Li-rich layered oxides such as $\text{Li}_2\text{Ru}_{1-y}\text{Sn}_y\text{O}_3$ have been reported in the literature to cycle better even with the participation of O^{2-} ligand in the reversible redox process.²⁰

The general electrochemical behaviour of the compounds Li_3MRuO_5 described in this manuscript is similar to those reported previously for Li_3MRuO_5 and $\text{Li}_2\text{M}_2\text{RuO}_6$ with $\text{M}=\text{Co}$ and Ni .^{3, 4} All of them exhibit the LiCoO_2 -type structure but $\text{Li}_3\text{MnRuO}_5$. The observed lithium electrochemical behaviour at low voltages (< 4.1) of all of them is determined just by the oxidation states of M and Ru atoms and their redox behaviour under lithium deinsertion/insertion. For example, in $\text{Li}_3\text{NiRuO}_5$ where nickel is Ni^{2+} and ruthenium Ru^{5+} , lithium deinsertion results mainly in oxidation of Ni^{2+} to Ni^{4+} ; in $\text{Li}_3\text{CoRuO}_5$, where cobalt is Co^{3+} but ruthenium Ru^{4+} , lithium deinsertion results in oxidation of Co^{3+} to Co^{4+} but also Ru^{4+} to Ru^{5+} , giving the observed electrochemical capacities. For $\text{Li}_3\text{MnRuO}_5$, where manganese is Mn^{3+} and ruthenium is Ru^{4+} (described in this manuscript), Mn^{3+} is oxidized to Mn^{4+} and Ru^{4+} to Ru^{5+} under lithium deinsertion. On the other hand, in $\text{Li}_3\text{FeRuO}_5$, where iron is Fe^{3+} and ruthenium is Ru^{4+} , lithium deinsertion results in oxidation of Ru^{4+} only; Fe^{3+} being stable does not seem to participate in the redox process.

Regarding the high voltage process, where the participation of oxygen may take place, the common behaviour is that in all the cases, O^{2-} seems to get oxidized to O^- like species under high voltages. The only difference with other described systems of the type Li_2MnO_3 - LiCoO_2 being the long life cycling behaviour. Among the Li_3MRuO_5 ($\text{M}=\text{Mn, Fe, Co}$ and Ni) compounds, $\text{Li}_3\text{NiRuO}_5$ and $\text{Li}_3\text{CoRuO}_5$ present higher reversibility capacity (ca. 200 mAh g^{-1}). Very recently the origin of voltage decay in high capacity layered oxides has been investigated on $\text{Li}_2\text{Ru}_1-y\text{Ti}_y\text{O}_3$, $\text{Li}_2\text{Ru}_{1-y}\text{Sn}_y\text{O}_3$ and Li_2RuO_3 unveiling a relationship with ionic sizes of cations. The slowest decay occurs for the largest cationic sizes.³⁵ However, in our case little difference in size can be found between the different investigated compounds. Interestingly, the disorder which is invariably present in all the lithium-rich rocksalt-type oxides seems to provide additional pathways for Li-diffusion (which are absent in well-ordered structures) and hence a higher rate capacity.^{1, 36} Thus, this supports our good results in the systems Li_3MRuO_5 $\text{M}=\text{Co}$ and Ni contrarily to the case of Mn . However, according to this, better results would be then expected for $\text{M}=\text{Fe}$ which was not observed, probably because Fe^{3+} is stable and does not get oxidized further under the electrochemical conditions investigated.

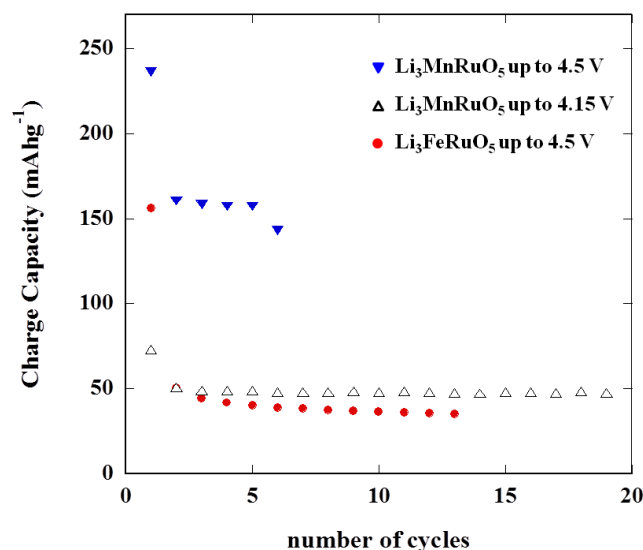


Fig 13 Charge capacity variation with cycle number for Li_3RuMO_5 ($\text{M} = \text{Mn}$ and Fe) in the 3.0 - 4.5 V voltage range. In the case of $\text{Li}_3\text{RuMnO}_5$ cycling in the 3.0 and 4.15 V range is also shown

Conclusions

New lithium-rich layered oxides with composition Li_3MRuO_5 ($\text{M} = \text{Mn}$ and Fe) have been synthesized for the first time. Crystal structure, magnetic properties, and lithium deinsertion/insertion electrochemistry have been investigated for $\text{M}=\text{Mn}$ and Fe . Li_3MRuO_5 is related to Li_2MnO_3 ($C2/m$) and LiCoO_2 ($R-3m$). In both structures, Li and $(\text{Li}_{0.2}\text{M}_{0.4}\text{Ru}_{0.4})$ layers are stacked alternately along the c -axis. Magnetic measurements indicate the presence of Mn^{3+} and low spin configuration for Ru^{4+} in $\text{Li}_3\text{MnRuO}_5$, where the Ru^{4+} itinerant electrons are occupying a π^* -band. The onset of a net maximum in the χ vs. T plot at 9.5 K and the negative value of the Weiss constant (θ) of -31.4 K indicate the presence of antiferromagnetic superexchange interactions according to different pathways. The Fe analogue oxide may have the same behaviour at low temperature since the onset of a net maximum at 20 K has been observed as in the case of the analogous manganese compound. Lithium electrochemical studies show a similar behaviour for both oxides and related to other Li-rich layered oxides in general. In both cases, a long first charge is observed. The corresponding capacities (240 mAhg^{-1} , 2.3 Li/f.u. and 144 mAhg^{-1} , 1.38 Li/f.u. for $\text{M} = \text{Mn}$ and Fe , respectively) indicate that not only the transition metals are participating in the redox chemistry. An initial sloping region (OCV ca. 4.1 V) is followed by a long plateau (ca. 4.3 V). Further discharge-charge cycling points to partial reversibility (ca. 160 and 45 mAhg^{-1} for Mn and Fe , respectively). XPS characterisation of both the pristine and electrochemically oxidized $\text{Li}_3\text{MnRuO}_5$ samples reveals that Mn^{3+} and Ru^{4+} are partially oxidized to Mn^{4+} and Ru^{5+} in the sloping region at low voltage, while in the long plateau O^{2-} is also oxidized to O^- related species. Oxygen release likely occurs and it is pointed out that this could be the origin of cells' failure on cycling. In $\text{Li}_3\text{FeRuO}_5$ the oxidation process appears to affect only Ru^{4+} (sloping region) and O^{2-} (plateau), while Fe seems to retain its 3+ state.

Acknowledgements

The authors are indebted to the Spanish Ministerio de Ciencia e Innovación (MICINN, Dirección General de Cooperación Internacional) for awarding and funding the Joint project ACI2009-0972 which made possible this work. Partial financial support coming from projects MAT2010-19837-C06, MAT2013-46452-C4-1-R, MAT2010-19460 (MICINN) and from the program S2009/PPQ-1626 (Comunidad de Madrid) is also acknowledged. On the other hand, J.G. and S.N. thank the Department of Science and Technology, Govt. of India for the award of Indo-Spanish project and Ramanna Fellowship.

Notes and references

- ^a *Solid State and Structural Chemistry Unit, Indian Institute of Science, Bangalore 560012, India. E-mail: gopal@sscu.iisc.ernet.in*
- ^b *Departamento de Química Inorgánica, Facultad de Ciencias Químicas, Universidad Complutense de Madrid, 28040 Madrid, Spain.*
- ^c *Departamento de Química y Bioquímica, Facultad de Farmacia, Universidad CEU San Pablo, 28668 Boadilla del Monte, Madrid, Spain.*
- ^d *E-mail: flaga@ceu.es*
- † Electronic Supplementary Information (ESI) available: [details of any supplementary information available should be included here]. See DOI: 10.1039/b000000x/
- ‡ Footnotes should appear here. These might include comments relevant to but not central to the matter under discussion, limited experimental and spectral data, and crystallographic data.
1. J. Lee, A. Urban, X. Li, D. Su, G. Hautier and G. Ceder, *Science*, 2014, **343**, 519-522.
 2. B. C. Melot and J. M. Tarascon, *Accounts of Chemical Research*, 2013, **46**, 1226-1238.
 3. S. Laha, E. Moran, R. Saez-Puche, M. A. Alario-Franco, A. J. Dos santos-Garcia, E. Gonzalo, A. Kuhn, S. Natarajan, J. Gopalakrishnan and F. Garcia-Alvarado, *Journal of Materials Chemistry A*, 2013, **1**, 10686-10692.
 4. S. Laha, E. Morán, R. Sáez-Puche, M. Á. Alario-Franco, A. J. Dos santos-Garcia, E. Gonzalo, A. Kuhn, F. García-Alvarado, T. Sivakumar, S. Tamilarasan, S. Natarajan and J. Gopalakrishnan, *Journal of Solid State Chemistry*, 2013, **203**, 160-165.
 5. Q. Q. Qiao, H. Z. Zhang, G. R. Li, S. H. Ye, C. W. Wang and X. P. Gao, *Journal of Materials Chemistry A*, 2013, **1**, 5262-5268.
 6. A. Alexander, P. D. Battle, J. C. Burley, D. J. Gallon and C. P. Grey, *Journal of Materials Chemistry*, 2003, **13**, 2612-2616.
 7. A. C. Larson and R. B. Von Dreele, *Los Alamos National Laboratory Report LAUR*, 2000, **86**.
 8. W. Kraus and G. Nolze, *Journal of Applied Crystallography*, 1996, **29**, 301-303.
 9. P. Strobel and B. Lambert-Andron, *Journal of Solid State Chemistry*, 1988, **75**, 90-98.
 10. H. J. Orman and P. J. Wiseman, *Acta Crystallographica Section C-Crystal Structure Communications*, 1984, **40**, 12-14.
 11. R. D. Shannon, *Acta Crystallographica Section A*, 1976, **32**, 751-767.
 12. R. I. Dass, J. Q. Yan and J. B. Goodenough, *Physical Review B*, 2004, **69**, 094416.

13. U. Manju, V. P. S. Awana, H. Kishan and D. D. Sarma, *Physical Review B*, 2006, **74**, 245106.
14. K. M. Shaju, K. V. Ramanujachary, S. E. Lofland, G. V. S. Rao and B. V. R. Chowdari, *Journal of Materials Chemistry*, 2003, **13**, 2633-2640.
15. T. Yamashita and P. Hayes, *Applied Surface Science*, 2008, **254**, 2441-2449.
16. J. C. Dupin, D. Gonbeau, P. Vinatier and A. Levasseur, *Physical Chemistry Chemical Physics*, 2000, **2**, 1319-1324.
17. R. Dedryvere, D. Foix, S. Franger, S. Patoux, L. Daniel and D. Gonbeau, *Journal of Physical Chemistry C*, 2010, **114**, 10999-11008.
18. T. Ohzuku and Y. Makimura, *Chemistry Letters*, 2001, 642-643.
19. M. Sathiya, K. Ramesha, G. Rousse, D. Foix, D. Gonbeau, A. S. Prakash, M. L. Doublet, K. Hemalatha and J. M. Tarascon, *Chemistry of Materials*, 2013, **25**, 1121-1131.
20. M. Sathiya, G. Rousse, K. Ramesha, C. P. Laisa, H. Vezin, M. T. Sougrati, M. L. Doublet, D. Foix, D. Gonbeau, W. Walker, A. S. Prakash, M. Ben Hassine, L. Dupont and J. M. Tarascon, *Nature Materials*, 2013, **12**, 827-835.
21. T. A. Arunkumar, Y. Wu and A. Manthiram, *Chemistry of Materials*, 2007, **19**, 3067-3073.
22. Y. Wu and A. Manthiram, *Electrochemical and Solid State Letters*, 2006, **9**, A221-A224.
23. A. R. Armstrong, M. Holzapfel, P. Novak, C. S. Johnson, S.-H. Kang, M. M. Thackeray and P. G. Bruce, *Journal of the American Chemical Society*, 2006, **128**, 8694-8698.
24. K. Numata, C. Sakaki and S. Yamanaka, *Solid State Ionics*, 1999, **117**, 257-263.
25. K. Numata and S. Yamanaka, *Solid State Ionics*, 1999, **118**, 117-120.
26. Z. H. Lu, L. Y. Beaulieu, R. A. Donabarger, C. L. Thomas and J. R. Dahn, *Journal of the Electrochemical Society*, 2002, **149**, A778-A791.
27. Z. H. Lu and J. R. Dahn, *Journal of the Electrochemical Society*, 2002, **149**, A1454-A1459.
28. Z. H. Lu and J. R. Dahn, *Journal of the Electrochemical Society*, 2002, **149**, A815-A822.
29. T. Ohzuku, M. Kitagawa and T. Hirai, *Journal of the Electrochemical Society*, 1990, **137**, 769-775.
30. J. M. Tarascon and D. Guyomard, *Journal of the Electrochemical Society*, 1991, **138**, 2864-2868.
31. M. M. Thackeray, P. J. Johnson, L. A. Depicciotto, P. G. Bruce and J. B. Goodenough, *Materials Research Bulletin*, 1984, **19**, 179-187.
32. J. M. Tarascon, G. Vaughan, Y. Chabre, L. Seguin, M. Anne, P. Strobel and G. Amatucci, *Journal of Solid State Chemistry*, 1999, **147**, 410-420.
33. L. Daheron, R. Dedryvere, H. Martinez, M. Menetrier, C. Denage, C. Delmas and D. Gonbeau, *Chemistry of Materials*, 2008, **20**, 583-590.
34. C. M. Julien and A. Mauger, *Ionics*, 2013, **19**, 951-988.
35. M. Sathiya, A. M. Abakumov, D. Foix, G. Rousse, K. Ramesha, M. Saubanère, M. L. Doublet, H. Vezin, C. P. Laisa, A. S. Prakash, D. Gonbeau, G. VanTendeloo and J. M. Tarascon, *Nat Mater*, 2014, **advance online publication** (DOI: 10.1038/NMAT4137).

-
36. A. Urban, J. Lee and G. Ceder, *Advanced Energy Materials*, 2014, **4**, 1400478